

pubs.acs.org/JACS Article

Perfect and Defective ¹³C-Furan-Derived Nanothreads from Modest-Pressure Synthesis Analyzed by ¹³C NMR

Bryan S. Matsuura, Steven Huss, Zhaoxi Zheng, Shichen Yuan, Tao Wang, Bo Chen, John V. Badding, Dirk Trauner, Elizabeth Elacqua, Adri C. T. van Duin, Vincent H. Crespi, and Klaus Schmidt-Rohr*



Cite This: J. Am. Chem. Soc. 2021, 143, 9529–9542



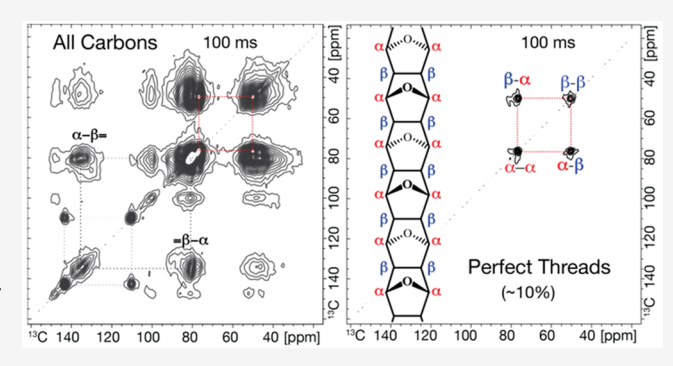
ACCESS

III Metrics & More

Article Recommendations

Supporting Information

ABSTRACT: The molecular structure of nanothreads produced by the slow compression of $^{13}\text{C}_4$ -furan was studied by advanced solid-state NMR. Spectral editing showed that >95% of carbon atoms were bonded to one hydrogen (C—H) and that there were 2–4% CH₂, 0.6% C=O, and <0.3% CH₃ groups. Alkenes accounted for 18% of the CH moieties, while trapped, unreacted furan made up 7%. Two-dimensional (2D) $^{13}\text{C}-^{13}\text{C}$ and $^{1}\text{H}-^{13}\text{C}$ NMR identified 12% of all carbon in asymmetric O—CH=CH—CH—CH—CH—and 24% in symmetric O—CH—CH—CH—CH—rings. While the former represented defects or chain ends, some of the latter appeared to form repeating thread segments. Around 10% of carbon atoms were found in highly ordered, fully saturated



nanothread segments. Unusually slow ¹³C spin-exchange with sites outside the perfect thread segments documented a length of at least 14 bonds; the small width of the perfect-thread signals also implied a fairly long, regular structure. Carbons in the perfect threads underwent relatively slow spin—lattice relaxation, indicating slow spin exchange with other threads and smaller amplitude motions. Through partial inversion recovery, the signals of the perfect threads were observed and analyzed selectively. Previously considered *syn*-threads with four different C—H bond orientations were ruled out by centerband-only detection of exchange NMR, which was, on the contrary, consistent with *anti*-threads. The observed ¹³C chemical shifts were matched well by quantum-chemical calculations for *anti*-threads but not for more complex structures like *syn/anti*-threads. These observations represent the first direct determination of the atomic-level structure of fully saturated nanothreads.

INTRODUCTION

Carbon's ability to form highly directional bonds in several different hybridizations yields a diverse panoply of molecular frameworks in zero, one, two, and three dimensions, including adamantanes, 1,2 fullerenes, 3,4 nanotubes, 5,6 nanohoops, 7 graphene, 10 graphane, 11,12 covalent organic frameworks, 13-15 and their ultimate ancestors graphite and diamond; these have garnered justifiably broad and deep interest in the scientific community. Saturated carbon nanothreads, which fill the onedimension/sp3 entry in this matrix of dimensionality and hybridization, were first synthesized by the high-pressure solid-state polymerization of benzene. Since then, a wide variety of nanothreads consisting primarily of sp³-hybridized carbon have been synthesized by the pressure-induced polymerization of aromatic molecules (e.g., pyridine, thiophene, and aniline), 18-22 co-crystals (e.g., naphthalene-octafluoronaphthalene, phenol-pentafluorophenol), 23-27 and a strained saturated hydrocarbon, cubane.²⁸ Pressure-induced solid-state reactions thus appear to be a general means of obtaining ordered packings of one-dimensional, high-aspect ratio diamond-like polymeric backbones decorated with diverse heteroatoms and functional groups, living at the threshold of thickness where

framework rigidity first emerges in solids, a regime rife with promise for novel chemical and physical properties. ^{29–32} Compared to solution-based organic synthesis, pressure-mediated solid-state synthesis is an underexplored method that provides access to new reaction pathways and products such as nanothreads that are unavailable or more challenging at ambient pressure. Advances in our understanding of nanothread synthesis—including the roles of temperature, ^{19,21} aromaticity, ²² molecular stacking geometry, ^{23–26} compression rate, ^{16,17,22,24} and uniaxiality of stress ^{16,17,20,22}—have been accompanied by substantial reductions in synthesis pressure, convincing demonstrations of sp³ character, ^{33,18–22} and initial ascertainments of axial periodicity²⁷ but not yet by a clear determination of the precise atomic structure of regular, periodic regions of saturated thread backbone.

Received: April 7, 2021 Published: June 15, 2021





Furan-derived nanothreads were recently synthesized at moderate pressure.²² Considering all synthetic organic methodologies (e.g., solution-based, solid-state, high-pressure synthesis, etc.), polymers synthesized in solution from furanbased monomers are well-known. Despite the prominence of poly(furan)s and complex furan-derived materials, 34,35 pressure-induced polymerization is currently the only known method to reliably achieve furan-derived nanothreads.²² The analogy to nanothreads in solution-state Diels-Alder polymerizations is close, but the resulting ladder polymers^{36,37} limited in both length and order. In contrast, mass spectrometry of pressure-synthesized nanothreads indicates molecular weights of about 6 kDa, consistent with ~100 furan units in the backbone. However, the detailed molecular structure has to date only been constrained by inferences as to the cross-sectional shape that follow from the detailed analysis of their crystalline packing.²² Three structures based on [4 + 2] cycloaddition pathways have been proposed, varying in the relative placement of oxygen atoms down the nanothread axis (see Figure 1). These threads were termed syn,

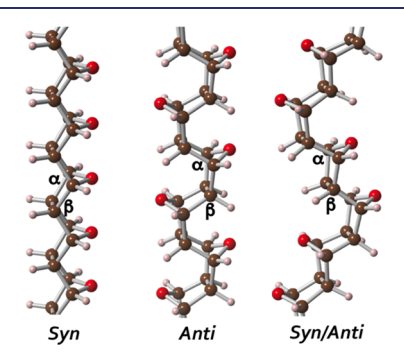


Figure 1. Syn-, anti-, and syn/anti-furan-derived nanothreads that can be formed through [4+2] cycloaddition. Examples of C_{α} (bonded to O) and C_{β} are marked in each structure.

anti, and syn/anti, wherein syn has eclipsed oxygens and anti has oxygen atoms alternating across the thread backbone. The intermediate syn/anti-case has oxygen atoms alternating in pairs. After slow decompression from 15 to 1.5 GPa, a sharp 6-fold diffraction pattern is observed in situ. A comparison of the experimentally observed d-spacings of Friedel pairs to those obtained from atomistic simulations of the proposed structures suggested anti and syn/anti as candidate structures but could

not distinguish between them or variants thereof.²² Molecular-level information of sufficient fidelity to determine a precise nanothread structure below the current resolution limit of electron microscopy in these systems and beyond the information so-far obtained from XRD has been lacking to date for any nanothread type. Here, we report solid-state NMR measurements of isotopically enriched furan-derived nanothreads that answer this call.

Solid-state NMR provides unique opportunities for a comprehensive and quantitative structural analysis of complex organic materials like nanothreads on the molecular level. 33 It takes advantage of structurally characteristic ¹³C and ¹H chemical shifts, which are also amenable to quantum-chemical simulations.³⁸ Unlike in vibrational spectra, peak areas in NMR are quantitative if the experiment has been performed appropriately, which means that the relative concentrations of different moieties can be determined. Modern NMR involves much more than just taking "the" $^{\rm 13}C$ NMR spectrum. Spectral editing, e.g., in terms of the number of hydrogen atoms attached to a given carbon, ³⁹ assists in peak assignment. Two-dimensional ¹H-¹³C spectroscopy with homonuclear ¹H decoupling provides access to the ¹H chemical shifts and with ¹H spin diffusion enables domain-size analysis on the 10 nm scale. Mobile segments can be identified through motional averaging of orientation-dependent spin interactions or characteristic changes in spin-relaxation times. 40 Materials made from ¹³C-enriched precursors provide many additional opportunities. 33 The 90-fold enrichment over the natural 13 C abundance of 1.1% provides a 90-fold signal enhancement that enables the detection of C=O, CH₃, and other spectrally resolved moieties down to a level of 0.1% of all C. With a ¹³C spin in every carbon site, strong one-bond ¹³C-¹³C couplings can be exploited in two-dimensional ¹³C-¹³C NMR to determine which carbons are bonded or separated by a few bonds.33 Through multistep 13C spin exchange or spin diffusion, proximities or domains on the scale of several nanometers can be probed. In crystalline or otherwise highly ordered systems, the number of carbons in the local asymmetric unit cell (e.g., the number of differently oriented C—H bonds in nanothreads) can be determined by centerband-only detection of exchange (CODEX) NMR⁴¹ with ¹³C spin exchange.

Scheme 1. Synthesis of ¹³C₄-Furan

■ EXPERIMENTAL SECTION

Synthesis of ¹³C₄-Furan. As shown in Scheme 1, the synthesis of ¹³C-furan was achieved starting from commercially available ¹³C₃propargyl alcohol (2) using a modified procedure adapted from Vu et First, ¹³C₃-propargyl alcohol (2) was protected using the tetrahydropyranyl group under acidic conditions, affording 3 in quantitative yields. Following this, 3 was deprotonated with n-butyl lithium (n-BuLi), and the corresponding lithium acetylide was reacted with ¹³C-labeled formaldehyde, producing 4 in 96% yield, which was subsequently deprotected to ¹³C₄-butyn-1,4-diol (5) in moderate yield. The reported conditions for the semihydrogenation of 5 were unsatisfactory in our hands and prone to over reduction and alkene isomerization. These problems were circumvented by using modified conditions, reacting 5 with 8 wt % Lindlar's catalyst and 1.0 equiv of quinoline in methanol under a hydrogen atmosphere, affording $^{13}C_4$ -cis-buten-1,4-diol (6) in 84% yield. Although we were able to replicate the reported conditions for the final oxidative cyclization, we found that it was unsuitable for use on a small scale. After considerable experimentation using biphasic conditions⁴⁴ or alternative oxidants such as Bobbitt's salt⁴⁵ or Dess-Martin periodinane, we found that heterogeneous conditions using substoichiometric pyridinium chlorochromate (PCC) in 6:1 water/H₂SO₄ could reliably generate ${}^{13}C_4$ -furan (1) in 25% yield after fractional distillation. The success of this subtle modification of the reported reaction conditions is presumably due to the poor aqueous solubility of PCC, which prevented the undesired overoxidation of 6. More details are given in the Supporting Information (SI, Section S4).

Modest-Pressure Synthesis of ¹³C-Furan-Derived Nanothreads. ¹³C₄-furan was loaded into an encapsulated stainless-steel gasket and slowly compressed and decompressed using a V7 Paris-Edinburgh press (PE Press) equipped with double-toroid polycrystalline diamond anvils.⁴⁷ Liquid nitrogen was used to freeze the liquid ¹³C-enriched furan into a solid to ensure that the gasket was completely filled without any trapped air; the evaporated nitrogen gas also helped to exclude water and oxygen from the loading container. The system was driven by an automatic oil syringe pump, allowing for controllable pressure ramp rates. A pressure-load calibration curve was used from previously reported data for the double-toroid anvil design.⁴⁸ The sample pressure was approximately 17 GPa at an oil pressure of 807 bar. When the oil pressure reached 547 bar, a slow rate of increase (1 bar/min) was employed in both compression and decompression cycles. Approximately 4 mg of solid was produced from 21 µL of ¹³C₄-furan loaded into the gasket.

Basic Solid-State NMR Parameters. Solid-state NMR experiments were performed on a Bruker Avance Neo 400WB NMR spectrometer at ¹H and ¹³C resonance frequencies of 400 and 100 MHz, respectively. Most of the measurements were conducted using a Bruker double-resonance magic-angle-spinning (MAS) probe with 4 mm zirconia rotors. Approximately 4 mg of ¹³C furan-derived nanothread sample as received was center-packed into the rotor. The empty space at the bottom of the rotor was filled by glass-fiber wool and a glass spacer, while a small disk made of Teflon tape was used to cap the sample. The 90° pulse strengths for 1H and ^{13}C were $|\gamma B_1|/2\pi$ = 69 and 62 kHz, respectively. Two-pulse phase modulation $(TPPM)^{49}$ ¹H decoupling at a field strength of $|\gamma B_1|/2\pi = 95$ kHz was used during the Hahn echo⁵⁰ or the total suppression of sidebands (TOSS)⁵¹ for dead-time-free detection, while ¹H decoupling by SPINAL-64⁵² at $|\gamma B_1|/2\pi = 85$ kHz was applied during signal acquisition. ¹³C chemical shifts were referenced externally to tetramethylsilane (TMS) using the carboxyl resonance of α -1-¹³Cglycine at 176.49 ppm as a secondary reference. The sample temperature during the NMR experiments at 5.787 kHz MAS was around 295 K, while it was raised to approximately 313 K at 14 kHz MAS due to frictional heating.5

An acquisition time between 6.2 and 15.5 ms was typically used in the one-dimensional (1D) 13 C NMR experiments. The 13 C B_1 field strength used in cross-polarization was optimized for each MAS frequency. Unless otherwise stated, the spectra presented were acquired with recycle delays ranging from 4 to 12 s at a MAS

frequency of 14 kHz. Quantitative ¹³C NMR spectra were measured using ¹³C direct polarization (DP) with a recycle delay of 80 s, averaging 576 scans (~21 h measuring time). Spinning sidebands occur at ±140 ppm from the corresponding centerband. They do not overlap with centerbands, since the range of centerband frequencies in this sample is 150 - 25 = 125 < 140 ppm. Cross-polarization (CP) MAS ¹³C NMR experiments were performed with a typical contact time of 1.1 ms and a 90-100% amplitude ramp on the ¹H channel. To exclude the possibility of highly crystalline furan-derived nanothreads with an extremely long T_{1H} , a CP experiment with a 3400 s recycle delay was conducted with 32 scans. The ¹³C spin-spin relaxation time (T_{2C}) was measured at 14 kHz MAS after CP using a Hahn spin echo ranging from 0.14 ms $(1 \times 2 t_r)$ to 3 ms $(21 \times 2 t_r)$. Peak intensities at 81 and 51 ppm were fitted with single exponential functions with time constants of $T_{2C} = 2.3$ and 2.2 s, respectively, corresponding to homogeneous full line widths at half-maximum of

One-pulse ¹H NMR spectra were measured with one-pulse probehead background suppression^{5,4} at 5 kHz with 64 scans and 15 s recycle delays, with the ¹H carrier frequency set at 2.5 ppm. ¹H chemical shifts were internally referenced to highly mobile furan doublets centered at 6.4 and 7.4 ppm.

¹³C NMR with Spectral Editing. Selective spectra of nonprotonated ¹³C or segments undergoing fast large-amplitude motions were recorded after direct polarization with 80 s recycle delays, using recoupled ¹H-¹³C dipolar dephasing, with ¹H decoupling switched off for 40 and 27 μ s before and after the echo π -pulse, respectively; compared to the conventional symmetric 2 \times 30 μ s gated decoupling, the residual signal was reduced by a factor of 0.7. A CH-only spectrum was obtained by dipolar distortionless enhancement by polarization transfer (dipolar DEPT) at 5787 Hz MAS;³⁹ 4096 scans were averaged for ~5 h. The CH₂-only spectrum was obtained by three-spin coherence selection⁵⁵ at 5787 Hz MAS with a CP contact time of 70 μ s and a carefully tuned flip-back pulse; 16384 scans were averaged for ~23 h. Hydroxyl-proton selected (HOPS) ¹³C NMR⁵ was performed to look for C-OH moieties in the 13C-enriched furan-derived nanothreads. The ¹H on-resonance frequency was set at 10.5 ppm for HOPS with a CP contact time of 0.25 ms; 1024 for both S and S_0 spectra were averaged within a total time of 3 h.

Spectra near the zero-crossing during 13 C inversion recovery 57 were recorded after CP to selectively observe components with different 13 C spin—lattice relaxation times (T_{1C}) . The pulse length of the inversion pulse after CP was reduced to 3 μ s for less complete magnetization inversion, resulting in an earlier zero-crossing of the recovering magnetization. Recovery times differing by \sim 2 s were used for the selective polarization of the perfect thread signals and other signals, respectively. The T_{1C} relaxation times slowly increased over a few weeks of measurements, probably due to a partial loss of trapped unreacted furan, which drives relaxation due to its large-amplitude mobility. For ease of illustration, the signal in some spectra using the inversion—recovery filter is shown inverted to display the negative, more slowly relaxing peaks as positive. For a standard 13 C inversion recovery experiment, 2816 scans were averaged over 12 h.

2D and Exchange ¹³**C NMR Experiments.** A two-dimensional (2D) double-quantum/single-quantum (DQ/SQ, solid-state INAD-EQUATE) ¹³**C** NMR spectrum was measured at 14 kHz MAS using the SPC5⁵⁸ ¹³C $^{-13}$ C dipolar recoupling sequence without ¹H irradiation for a duration of 2 × 0.29 ms, relying on ¹³C irradiation at $|\gamma B_1|/2\pi = 70$ kHz for heteronuclear decoupling. The total acquisition time was 69 h. Shearing of the DQ/SQ spectrum⁵⁹ to match the appearance of 2D exchange spectra was performed via the "ptilt1" functionality in Bruker TopSpin 4.0.4 using alpha1 = alpha2 = 0.5

Two-dimensional $^{1}H-^{13}C$ heteronuclear correlation (HetCor) 60 spectra were measured at a 7.5 kHz MAS frequency with frequency-switched Lee–Goldburg homonuclear ^{1}H decoupling 61 at $|\gamma B_{1}|/2\pi=85$ kHz and TOSS before detection. ^{1}H spin-diffusion was allowed to occur during a mixing time ranging from 10 μ s to 10 ms. For longer mixing times (3 and 10 ms), a CP contact time of 500 μ s was used, otherwise the CP contact time was 70 μ s. A typical spectrum was

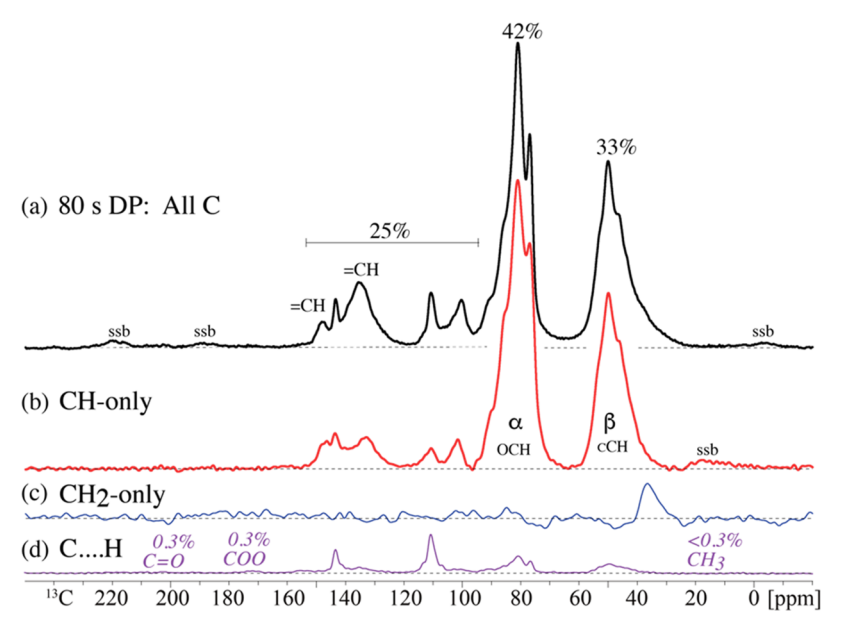


Figure 2. ¹³C NMR of ¹³C-furan-derived nanothreads with spectral editing. (a) Quantitative direct-polarization ¹³C NMR spectrum. (b) CH-only spectrum at 5787 Hz MAS. (c) CH₂-only spectrum. (d) Direct-polarization spectrum after recoupled dipolar dephasing, showing mobile furan but little signal of C not bonded to H or of CH₃ groups. "ssb": spinning sideband.

signal-averaged for 17-21 h (\sim 93 h total). The ACD/NMR Predictors⁶² were used to predict ^{1}H and ^{13}C chemical shifts in alkene-containing structures.

Two-dimensional ¹³C-¹³C exchange spectra were recorded at 14 kHz MAS with mixing times ranging from 10 ms to 1 s. For the experiment with a mixing time of 10 ms, dipolar assisted rotational resonance (DARR) by weak ¹H irradiation ⁶³ was used to promote ¹³C-¹³C spin-exchange. The measurement time per 2D spectrum was 12-21 h. For the selective observation of spin exchange among perfect-thread carbons, a mixing time of 100 ms was used in a 2D ¹³C-¹³C exchange spectrum after a 6 s ¹³C inversion recovery filter (~27 h of measurement time).

 $^{13}\mathrm{C}$ spin exchange out of the perfect thread segments was observed after 6.7 s of inversion recovery that suppresses the signals of the other threads, followed by a 36 $\mu\mathrm{s}$ chemical shift filter to suppress the total integral of the furan signals at 111 and 143 ppm, with the $^{13}\mathrm{C}$ carrier frequency set to 65 ppm. The chemical-shift filter was followed by a mixing time for $^{13}\mathrm{C}$ spin diffusion (ranging from 3 ms to 3 s) before detection. The pulse sequence for this experiment is shown in Figure S7. For each mixing time, S12 transients were averaged for ~ 15 h.

Centerband-only detection of exchange (CODEX) NMR experiments 41 for probing $^{13}\mathrm{C}$ spin exchange were performed at a 14 kHz MAS frequency. It was confirmed experimentally that $Nt_{\rm r}=1.14$ ms (with 2 \times 15 π -pulses) produced a well-dephased S spectrum in the long-time limit. The $^{13}\mathrm{C}-^{13}\mathrm{C}$ spin-exchange/diffusion along the threads was probed using 10 mixing times ranging from 2 ms to 1 s. The total experimental time for all the CODEX experiments was $\sim\!20$ h. An 8.5 s $^{13}\mathrm{C}$ inversion recovery filter was applied before the CODEX evolution period to selectively probe the spin-diffusion behavior of the perfect threads, for four mixing times, requiring a total of $\sim\!7$ days of signal averaging. Spin-exchange dynamics were simulated in MATLAB as outlined in the SI.

Quantum–Chemical Simulations. The NMR chemical shielding tensors of carbon in furan-derived syn-, anti-, syn/anti-, [2+2] polymer, and 1,3-polymer structures were calculated in the framework of density functional theory with the gauge-including projector augmented wave (GIPAW) method $^{64-67}$ implemented in Quantum ESPRESSO. 68 The GIPAW reconstructed pseudopotentials 69 with the Perdew–Burke–Ernzerhof (PBE) 70 functional utilizing the Troullier–Martins norm-conserving method were used for all calculations, with a 100 Ry energy cutoff and a <0.24 Å $^{-1}$ k-point spacing to obtain

converged NMR parameters at a reasonable computational cost. The isotropic chemical shift was calculated as 71,72

$$\delta_{\rm iso}^{\rm calc} = \frac{\sigma_{\rm iso}^{\rm ref} - \sigma_{\rm iso}^{\rm calc}}{1 - \sigma_{\rm iso}^{\rm ref}} \tag{1}$$

where $\sigma_{\rm iso}^{\rm calc}$ is the calculated isotropic chemical shielding and $\sigma_{\rm iso}^{\rm ref}$ is the reference isotropic chemical shielding. To minimize systematic errors, $\sigma_{\rm iso}^{\rm ref}$ was determined by linear fitting of the calculated isotropic chemical shielding values for several structurally related systems to their known experimental isotropic chemical shifts with the equation 38

$$-\sigma_{\rm iso}^{\rm calc} = m\delta_{\rm iso}^{\rm exp t} - \sigma_{\rm iso}^{\rm ref}$$

■ RESULTS

Quantitative ¹³C NMR. Figure 2a shows a quantitative, fully relaxed direct-polarization ¹³C NMR spectrum of ¹³C-enriched furan-derived nanothreads. It exhibits eight peak maxima and several shoulders. The structural moieties associated with these spectral features will be identified in the following through spectral editing, ¹H–¹³C, and, most importantly, two-dimensional ¹³C–¹³C NMR. Peak areas (also taking into account spinning sidebands) are quantitative. It is found that 25% of carbons resonate at \geq 100 ppm, which means that they are sp²-hybridized. The intensity of the alkyl β-carbons (C not bonded to O) is significantly lower than that of the α-carbon (OCH) peak. This initially unexpected asymmetry will be fully explained below in terms of a significant fraction of alkene β-carbons.

Spectral Editing in ¹³C NMR. A selective spectrum of CH groups (carbon atoms each bonded to one hydrogen), obtained by dipolar DEPT, is shown in Figure 2b. Most peaks are retained, as expected in furan-derived nanothreads. A CH₂-only spectrum obtained by three-spin coherence selection accordingly shows only one peak, near 38 ppm; the corresponding foot in the full spectrum represents 2–4% of the total intensity. The spectrum of carbons with weak dipolar couplings to H, obtained by recoupled dipolar dephasing and

shown in Figure 2d, exhibits little signal. Two sharp peaks are observed at the resonance frequencies of furan and can be assigned to trapped unreacted furan molecules with anisotropic mobility. With sufficient vertical expansion, COO and ketone bands of 0.3% signal fraction each can be recognized (see Figure S1). In total, the data show that >95% of all carbons are bonded to one hydrogen, which is a characteristic of nanothreads made from unsubstituted single aromatic rings. Due to an apparent OH band in the IR spectrum, ^{22,73} we searched for C—OH signals using hydroxyl-proton selection (HOPS) NMR, ⁵⁶ but no such signals were recognized (see Figure S2) above the detection limit of ~2%.

One-Bond 2D NMR: Alkene Identification. The =C-H signals between 100 and 150 ppm in the 13 C spectrum can be assigned on the basis of characteristic cross peaks in 2D 13 C $-^{13}$ C and 1 H $-^{13}$ C NMR spectra with mostly one-bond transfer. Figure 3 shows 13 C $-^{13}$ C spectra with one-bond and weak two-bond correlation peaks. Figure 3a is a DQ/SQ correlation spectrum analogous to an INADEQUATE spectrum in solution NMR but sheared to take the appearance

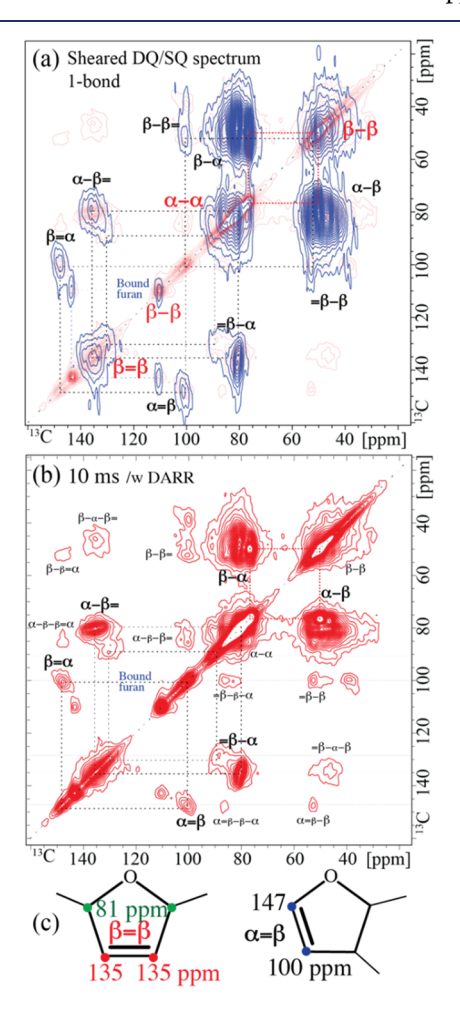


Figure 3. Two-dimensional $^{13}\text{C}-^{13}\text{C}$ NMR of ^{13}C -furan-derived nanothreads. (a) Sheared DQ/SQ spectrum. (b) Exchange spectrum with a 10 ms mixing time and the application of weak ^{1}H irradiation for dipolar assisted rotational resonance (DARR). This spectrum is also shown faintly in the background in (a). The labels " $\alpha-\alpha$ " and " $\beta-\beta$ " refer to true diagonal peaks in (a) and to near-diagonal cross peaks in (b). (c) Symmetric and asymmetric alkene-containing rings proven by diagonal peaks (or their absence) in (a) and cross peaks in (a) and (b).

of an exchange NMR spectrum with cross peaks,⁷⁴ matching the spectrum in Figure 3b. While the cross peaks in (a) are broader than those in (b), the diagonal peaks in (a) are highly valuable in showing that two carbons with very similar chemical shifts are bonded to each other, often indicating a symmetric structure (while the exchange spectrum in (b) contains meaningless diagonal peaks). Such signals of chemically equivalent spins are not observable in J-coupling-based INADEQUATE but are generated by the recoupled ¹³C-¹³C dipolar interaction in the solid state. For instance, two carbons with chemical shifts near 135 ppm are bonded to each other; in conjunction with the (135, 81 ppm) cross peak prominent in Figure 3 a,b, this proves a symmetric ring structure with a C_{β} C_{β} double bond (see Figure 3c). The directly bonded β carbons of the trapped furan also give rise to a clear diagonal peak near 111 ppm. Strong cross peaks between 147 and 100 ppm prove there is an O— $C_{\alpha}H$ = $C_{\beta}H$ — fragment (see Figure 3c); since it is in an asymmetric ring structure (after all, the symmetric structure would be an isolated furan ring), it does not have associated diagonal peaks in Figure 3a.

These alkene assignments can be confirmed in a $2D^{1}H^{-13}C$ NMR spectrum with short, one-bond cross-polarization from ^{1}H to ^{13}C (see Figure S3a), where the ^{1}H chemical shifts of the C=C—H units can be read off. Characteristic C=C ^{-1}H chemical shifts of 6.1 and 4.9 ppm were observed. The agreement with chemical shifts from empirical predictions using the ACD/NMR Predictors was good (see Figure S3b). The fractions of different sp 2 - and sp 3 -hybridized carbons are summarized in Table 1.

Alkyls near Alkenes. By extending the mixing time in spin-exchange 2D 13 C $^{-13}$ C NMR to 100 ms, we can probe site proximities over several bonds. The 100 ms exchange spectrum shown in Figure 4a has stronger long-range exchange peaks compared to the few-bond-transfer spectra in Figure 3. The peak positions can be assessed most conveniently in horizontal cross sections through the 2D spectrum (see examples in Figure 4b). These are equivalent to spectra obtained by selective excitation at the evolution frequency ω_1 (the position of the peak on the diagonal) followed by spin exchange during the mixing time, e.g., 100 ms here.

Selected horizontal cross sections through the 10 and 100 ms spectra (in blue and red, respectively) are shown in Figure 4b, with the diagonal-peak intensities matched for clarity. The biggest secondary peaks in the 10 ms spectrum are due to the one-bond couplings already discussed. Two- and three-bond transfer peaks are smaller in amplitude but are usually significantly enhanced after 100 ms of spin exchange. Some of the chemical shift assignments deduced are shown in the structures next to the spectra. The cross peaks from alkenes to OCH at 89, 86, and 81 ppm can account for shoulders and peaks in the complex OCH resonance, as indicated schematically in the 1D spectrum above the 2D spectrum in Figure 4a.

The cross peak labeled ' $=\beta-\alpha$ ' in Figure 4a exhibits at least two components: a narrow one at (135, 81 ppm) and a broader one at (\sim 128, 80–90 ppm). A comparison of the cross sections in Figure 4b labeled "135 ppm" and "128 ppm" makes the larger width of the 128 ppm cross peak even more apparent. This indicates a more varied bonding environment of the $C_\beta=C_\beta$ alkene resonating at 128 ppm, suggesting that it is a defect in a variety of thread environments. The 135 ppm of $C_\beta=C_\beta$ alkene appears to belong to a more specific bonding environment; the periodic structure made up of repeating,

Table 1. Composition of ¹³C-Furan-Derived Nanothreads in Terms of Carbon Percentages (of the segments highlighted in bold) and of Fractions of Furan-Ring Equivalents

Moiety	C=O	COO	Furan	H-C C-H	н-с О.с-н	Anti	Other	CH ₂
			C ₄ H ₄ O	н-с=с-н	н-с-с-н	sp ³ -CH		
% of C	0.3%	0.3%	7%	12%	6%	10%	61%	3±1%
% of rings	N/A	N/A	7%	24%	12%	10%	46%	N/A
			±2%	±2%	±2%	±3%	±5%	

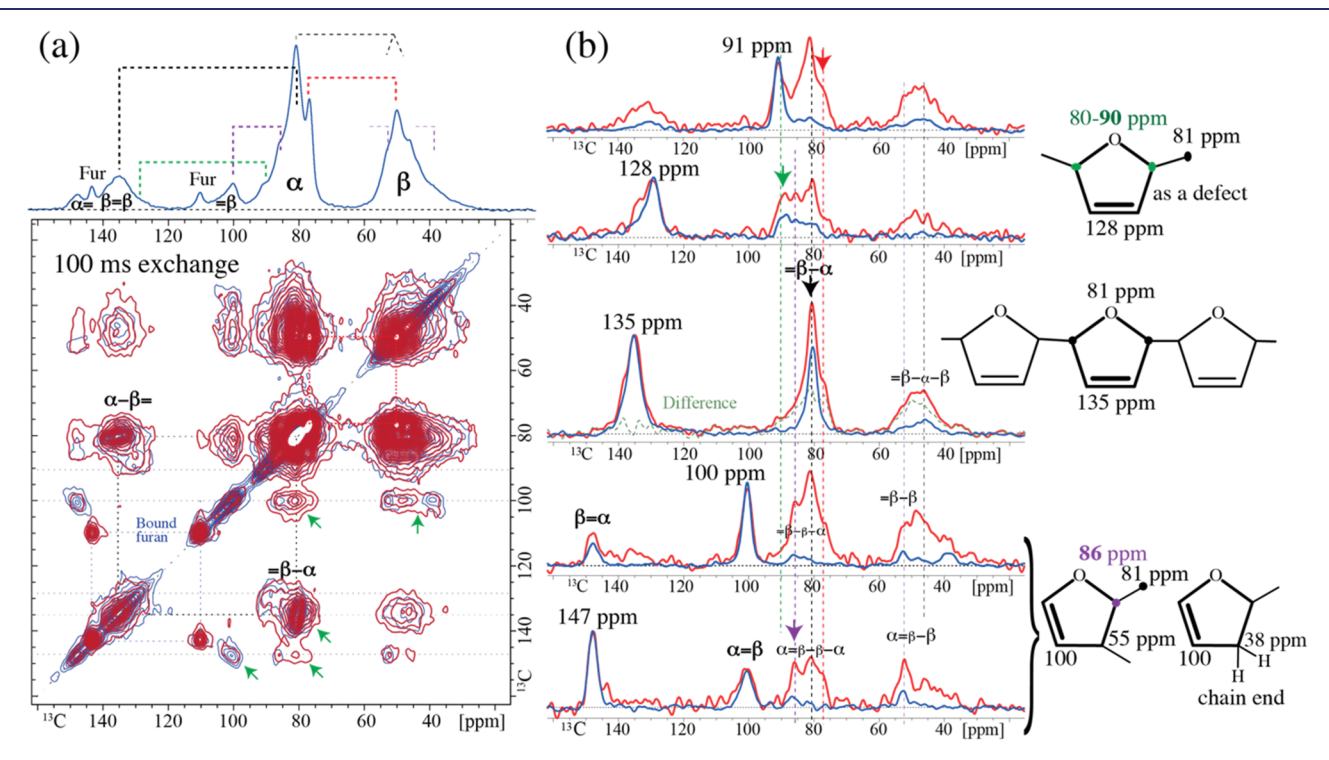


Figure 4. Few-bond connectivity of ¹³C-furan-derived nanothreads. (a) 2D exchange spectra with 100 ms mixing time (red) and 10 ms (thin blue) overlaid, and (b) horizontal cross sections from the spectra in (a), with the intensities of the diagonal peaks matched. In the top-left spectrum, the assignments of peaks and shoulders of the OCH peak are indicated schematically.

symmetric alkene-containing rings shown in Figure 4b, center, is a good candidate.

Perfect-Thread Signals in 2D ¹³C—¹³C NMR Spectra. The analysis so far has mostly focused on the relatively low peaks associated with the various types of alkenes. Interesting features also become apparent in the alkyl—alkyl correlation region when the 100 ms 2D exchange spectrum, processed with minimum digital line broadening, is plotted at much higher contour levels (see Figure 5a). The graph reveals an intriguing set of four sharp peaks arranged in a square, superimposed on broader and mostly lower signals. The four sharp peaks of similar intensity are indicative of exchange within a highly symmetric and repetitive environment containing just two chemically inequivalent sites, CH and OCH, with chemical shifts of 50 and 77 ppm, respectively. We refer to these as "perfect threads" in the following.

On the basis of their slower inversion recovery, described in the following, the 2D spectrum of the perfect threads can be observed selectively (see Figure 5b). Cross sections at the 50 and 77 ppm frequencies (also in Figure 5b) show the two peaks in a 1:1 ratio, as expected for simple, fully saturated furan-derived nanothreads, without much cross-talk to other carbon sites.

The bonding in the perfect threads can be determined by analyzing their signals in the sheared DQ/SQ spectrum as plotted in Figure S4. Strong C_{α} — C_{β} cross peaks document predominant bond formation between a C_{α} of one ring and a C_{β} of a neighbor. While a C_{β} — C_{β} diagonal peak was also clearly observed and expected as a result for the C_{β} — C_{β} bond in furan, no significant C_{α} — C_{α} diagonal peak was observed, indicating the absence of C_{α} — C_{α} bonding in the perfect threads. The round, narrow C_{α} — C_{α} diagonal peak after 100 ms of 13 C spin exchange in Figure 5b can be attributed to exchange between chemically equivalent C_{α} sites separated by two bonds in the periodic perfect threads.

The perfect threads also stand out in an exchange spectrum with an even longer mixing time of 1000 ms (see Figure S5). All other nanothread sites reach spin-exchange equilibrium: regardless of their initial frequency along the vertical axis, the magnetization distributes over all types of carbon in their representative proportions, which means that an equilibrated horizontal cross section is a scaled version of the unselective one-dimensional spectrum. This is the case at all frequencies except 50 and 77 ppm, where the peaks of the perfect threads remain enhanced because they have not shared most of their magnetization with other carbon sites.

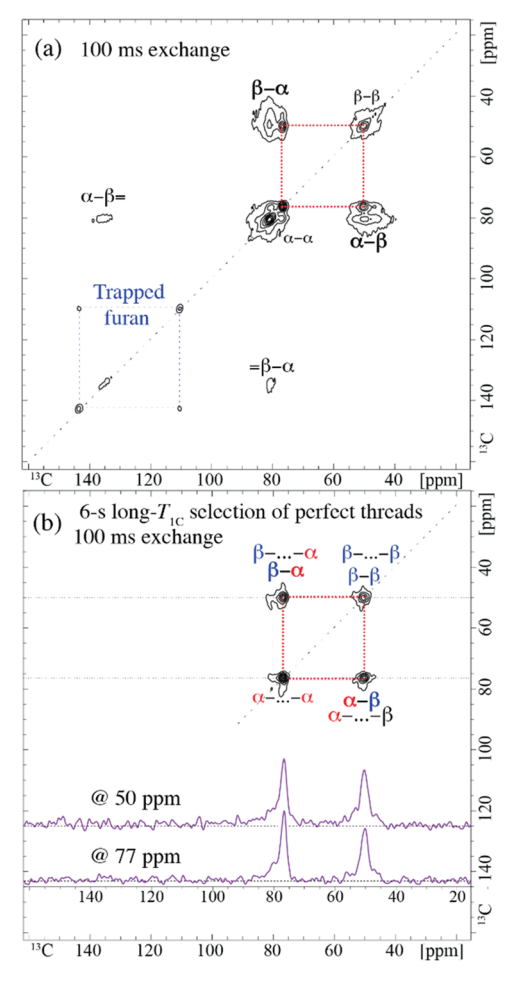


Figure 5. Two-dimensional $^{13}\text{C}-^{13}\text{C}$ exchange NMR spectra of ^{13}C -furan-derived nanothreads, highlighting signals of perfect threads. (a) Exchange NMR with a 100 ms mixing time (same data as in Figure 4a, but without digital smoothing and plotted at higher contour levels). (b) Same after a selection of the longest- $T_{1\text{C}}$ component by 6 s inversion recovery. Horizontal cross sections along the dashed lines are also shown.

Slower Inversion Recovery of Perfect-Thread Signals.

The selection of the perfect-thread signals is possible on the basis of their relatively slow $^{13}\mathrm{C}$ spin—lattice relaxation. While the standard methods of $T_{1\mathrm{C}}$ -selective spectroscopy, direct polarization with short recycle delay or phase-cycled z-filtering, were not discriminatory enough to cleanly separate the perfect-thread signals, the desired selection was achieved by inversion recovery timed such that the signal of the faster relaxing defective threads just passes through zero while that of the slower-relaxing perfect threads remains significantly inverted (see Figure 6). The signals of mobile trapped furan, which relax faster, have already passed through zero as they approach thermal equilibrium.

The observation that the sharp signals of the perfect threads relax the most slowly has at least two implications. First, it indicates a particularly long intrinsic $T_{\rm IC}$ relaxation time of the perfect threads, which in turn implies particularly limited molecular motion or less contact with a fast-relaxing mobile furan. Spin–lattice relaxation is driven by fluctuating magnetic fields, e.g., due to the orientation-dependent $^{13}C^{-1}H$ dipolar couplings made time dependent by molecular motions, specifically those with a spectral density at the nuclear Larmor

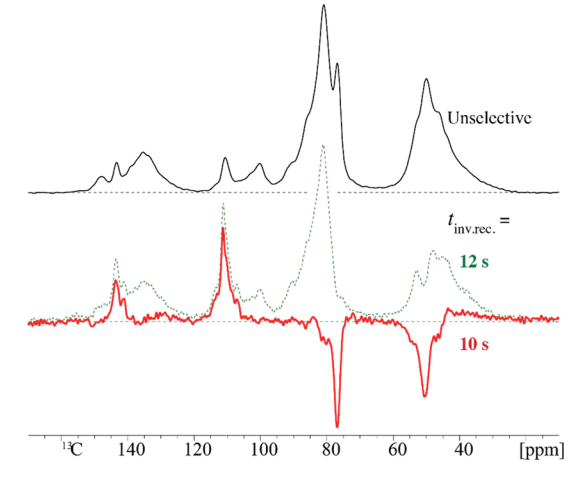


Figure 6. Spectra during ¹³C inversion recovery in ¹³C-furan-derived nanothreads, after (bottom red trace) 10 s and (middle dashed trace) 12 s of recovery time. An unselective DP spectrum, scaled to the same height of the 81 ppm peak, is shown at the top for reference.

frequency ($2\pi \times 100$ MHz here, corresponding to correlation times of a few nanoseconds). Most of the decrease in the relaxation rate of the perfect threads is likely due to a reduced motional amplitude, consistent with an ordered, ladder-type structure with little torsional flexibility.

The second implication is a significant length of a periodic structure containing only 50 and 77 ppm sites in a 1:1 ratio. During the multisecond recovery period after inversion, multistep 13C spin exchange occurs, as shown in Figure S8a,b and discussed in more detail below. If the segments containing the 50 and 77 ppm carbon sites were dispersed among the other alkyl and the alkene-containing structures, ¹³C-¹³C spin exchange would erase the effect of different intrinsic spin-lattice relaxation times and all segments would relax with the same time constant. The slow relaxation in the perfect threads raises the possibility that perfect threads in large crystallites might relax so slowly that their magnetization has only minimally recovered within the recycle delays of 6-80 s used in most of our experiments. This hypothesis was ruled out by cross-polarization ¹³C NMR with a 3400 s recycle delay, which showed no additional alkyl carbon signal (see Figure

Spin Exchange after Inversion Recovery. After inversion recovery to the zero crossing of the defective-thread signals, the spatial distribution of 13 C magnetization is in a state far from equilibrium. It will therefore undergo further 13 C spin exchange during a subsequent \pm z-filtered mixing time, with the spectrum slowly approaching the regular shape observed without selective excitation. The rate of decrease of the selected peaks is indicative of the length of the perfect thread segments. The total area under the signal is initially constant and then decreases exponentially toward zero as the mixing time increases, with the T_{1C} relaxation time as the time constant. The perfect-thread signal intensities can be corrected for the moderate reduction in overall signal due to relaxation.

In the selective spectrum of the perfect threads in Figure 6 (bottom), in addition to the desired negative signals of the slowly relaxing 77 and 50 ppm peaks, positive peaks of mobile furan were observed. These (specifically their combined overall intensity) can be reduced by a simple fixed evolution period of $36~\mu s$ between inversion recovery and additional spin exchange, which acts as a chemical shift filter. The resulting

sinusoidal excitation function is indicated dashed in Figure 7a. The furan peaks are reduced in intensity and have opposite

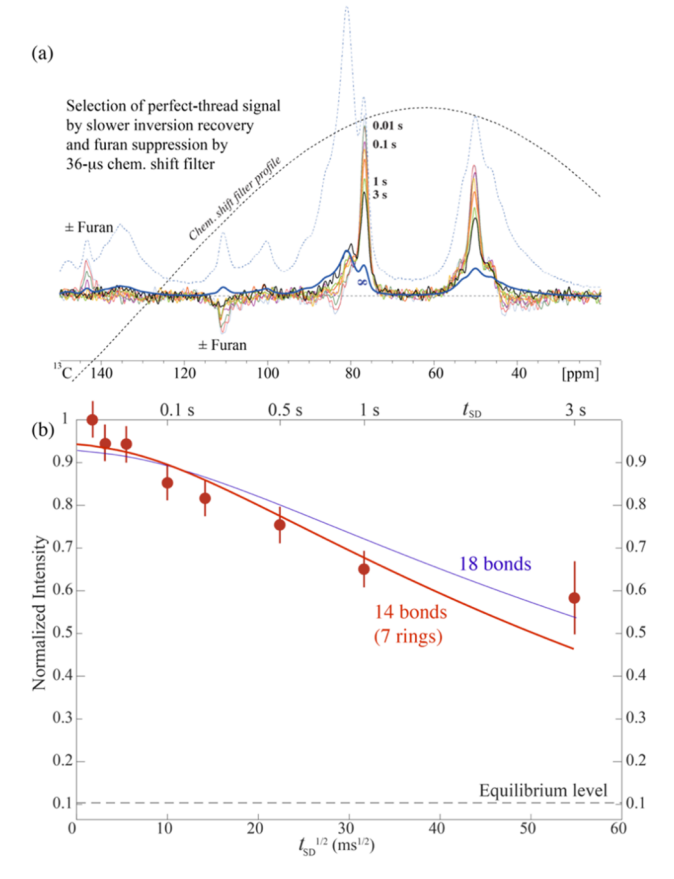


Figure 7. One-dimensional $^{13}\mathrm{C}$ spin-exchange experiment after inversion recovery and chemical-shift filtering that selects the magnetization of perfect thread segments in $^{13}\mathrm{C}$ -furan-derived nanothreads. The pulse sequence is shown in Figure S7. (a) Series of spectra as a function of mixing time. The excitation profile of the 36 μs chemical-shift filter aimed at suppressing the net magnetization of furan is shown by a dashed line. The full spectrum is also shown for reference at the top (faint dashed line) and scaled to the small area of the selective spectra (thick purple line). (b) Normalized intensity of the 77 ppm peak as a function of the square-root of the spin-exchange time. Thick red and thin blue lines: Fit curves for spin exchange after inversion recovery to the zero crossing of the matrix for perfect-thread segments that are 14 and 18 bonds in length, respectively.

signs, so the net magnetization in furan is very small and will not interfere with the spin exchange out of the perfect thread segments. The pulse sequence with all the mentioned elements is shown in Figure S7.

The series of spectra in Figure 7a shows the expected decay of the sharp perfect-thread signals with an increasing mixing time, toward the long-time equilibrium spectrum (the regular spectrum scaled to the same total area), which is also shown (thick blue line). The intensity of the sharp 77 ppm peak is plotted as a function of the square-root of the mixing time in Figure 7b. Two results of full simulation of inversion recovery with relaxation and spin diffusion, followed by further spin diffusion out of the perfect thread segments as discussed in the SI (see Figure S8c,d), are shown.

Quantum—Chemical Chemical Shift Prediction. The perfect threads show characteristic chemical shifts, in particular of the 77 ppm peak, which is quite well-resolved from most of

the other OCH signals. The fact that only two sharp peaks were observed is also structurally relevant. By comparison with chemical shifts from quantum-chemical simulations, one can rule out many structural models and identify the likely correct model. Figure 8 shows the structures of furan-derived syn-, anti-, and syn/anti-nanothreads, marked with the corresponding computed chemical shifts of symmetry-distinct carbons. The syn/anti-structure has four carbon sites with four distinct predicted chemical shifts of 79.7, 50.5, 83.7, and 54.4 ppm; this is clearly incompatible with the experimentally observed pair of peaks. This conclusion also applies by extension to other complicated nanothread structures. The syn-structure was computed to have chemical shifts of 87.2 and 49.0 ppm, deviating significantly from the observed 77 and 50 ppm. Only the computed peaks for anti-threads, at 79.3 and 49.6 ppm, are in good agreement with experiment. Note also that prior analysis of X-ray diffraction data on furan nanothread packing geometries strongly favors anti over syn, as the narrower and more uniform cross-section of syn-threads is not compatible with the experimentally observed Friedel spacings.²²

In addition to the syn- and anti-structures formed by [4 + 2]reactions, a product of [2 + 2] reactions and a 1,3-polymer⁷⁶ (see Figure 8, bottom) were also analyzed. Each contains two distinct C sites and eight distinct C-H orientations, so they are compatible with the experimental NMR results. The identification of one of these structures would have major implications for the nanothread formation mechanism. In structures optimized at the density functional based tightbinding (DFTB) level, the chemical shifts were 89.3 and 51.2 ppm for the [2 + 2] polymer and 81.5 and 44.4 ppm for the 1,3-polymer. These are clearly inconsistent with the experimental values of 77 and 50 ppm. To ensure that these discrepancies were not due to structural distortions, we also optimized the axial unit cell parameters for the two polymers at the DFT level. The chemical shifts changed only slightly to 90.3 and 51.4 ppm for the [2 + 2] polymer and 82.1 and 44.7 ppm for the 1,3-polymer. The discrepancy from the experimental values was not significantly reduced.

Counting Differently Oriented C—H Bonds in Perfect Threads. Advanced solid-state ¹³C NMR can also identify ordered ¹³C-enriched nanothreads on the basis of their symmetry. Straight *syn*-threads have the highest symmetry, with translation by one oxygen—oxygen distance along the thread axis leaving the structure unchanged; this means that there are only four differently oriented C—H bonds in this structure if it is straight and not twisted. In *anti*-threads, the structural period along the thread axis contains *eight* differently oriented C—H bonds, and in *syn/anti*-threads, the corresponding number is 12.

The number of differently oriented C—H bonds (technically, magnetically inequivalent sites) can be determined by centerband-only detection of exchange (CODEX) 13 C NMR, 41 taking advantage of 13 C— 13 C spin exchange. CODEX measures the intensity of a stimulated echo of the recoupled chemical-shift anisotropy for each resolvable isotropic chemical shift position. In the full dephasing limit, with a long enough recoupling time $Nt_{\rm r}$, the observed normalized intensity S/S_0 after the spin-exchange time is the fraction of magnetization in sites with the same C—H orientation as before the spin-exchange time; this is the inverse of the number of magnetically inequivalent sites. 41

Figure 9 shows the normalized intensity S/S_0 for the 81 ppm signal and for the 77 ppm peak in the perfect threads. The

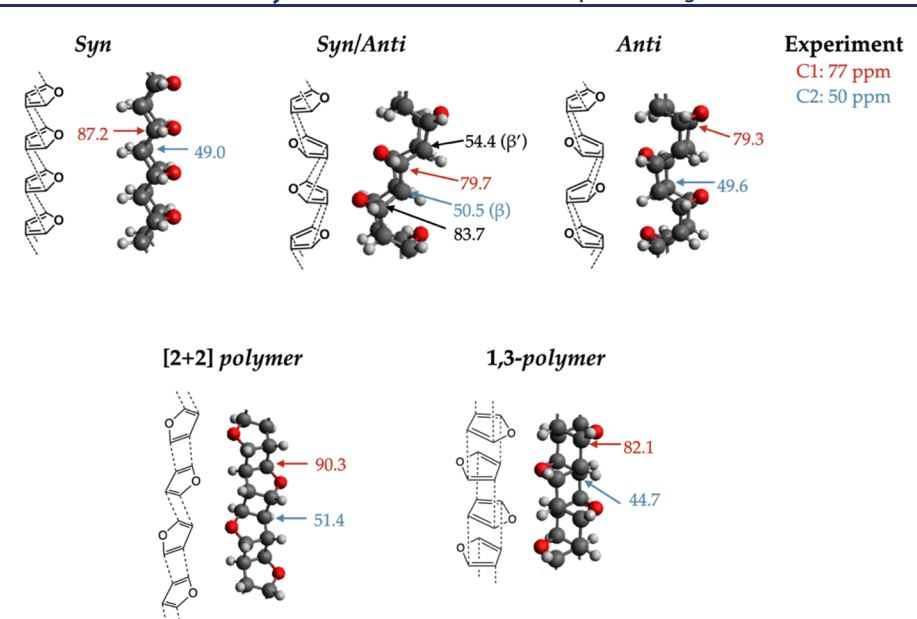


Figure 8. ¹³C chemical shifts, in parts per million, obtained from quantum-chemical simulations in five types of furan-derived nanothreads, demonstrating the close agreement of only *anti*-threads to the experimentally measured shifts.

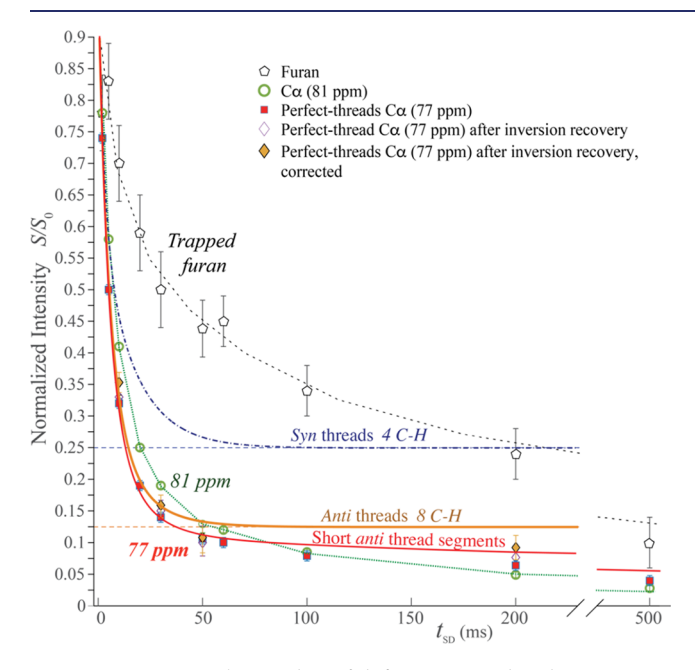


Figure 9. Counting the number of different C—H bond orientations in 13 C-furan-derived nanothreads by CODEX 13 C NMR. The plot shows the normalized CODEX signal intensity S/S_0 recorded at 81 ppm (open green circles), 77 ppm (filled red squares; perfect threads), and 143 ppm (open pentagons; trapped furan). Open orange diamonds: 77 ppm intensity after perfect-thread selection by inversion recovery. Filled orange diamonds: same as previous but corrected for the isotropic-chemical-shift exchange quantified in Figure 7b. Horizontal lines at 1/4 and 1/8 intensity indicate the equilibrium signal levels in straight syn- and anti-threads, respectively, while full spin-exchange simulations yielded the dash-dotted blue and the thick orange curves, respectively. Solid red curve: simulated CODEX decay for perfect anti-thread segments that are 14 bonds in length.

latter exhibits a faster initial decay, passing quickly through 0.25, the final level for straight *syn*-threads, and reaches a slowly decreasing equilibrium value near 1/8, the value for straight *anti*-threads. The simulation of ¹³C spin exchange in a

perfect-thread "ladder" structure with a one-bond exchange rate constant of k = 80 Hz (see the SI for details) produced the bold orange curve for *anti*-threads and the dash-dotted blue curve for *syn*-threads. The former provides an excellent fit to the data up to 50 ms. The additional slow signal decrease at >50 ms can be explained mostly by the finite length of the perfect thread segments: when magnetization diffuses out (see Figure S8e,f), there is a large change in chemical shift and corresponding loss of CODEX signal. Gradual twisting of the perfect *anti*-threads would also result in a loss of correlation of C—H bond orientations and CODEX intensity.

A comparison of the CODEX decays of OCH sites in perfect and defective threads in Figure 9 reveals distinctive differences. The perfect threads show a faster initial decay, which can be attributed to a more perfect "ladder" structure with two "parallel" $^{13}\mathrm{C}-^{13}\mathrm{C}$ couplings along the thread axis, while alkenes reduce the number of $^{13}\mathrm{C}-^{13}\mathrm{C}$ bonds in defective threads. At long times, the perfect threads show a slower decay than the matrix, indicating fewer differently oriented C—H bonds.

Probing the Size of Perfect-Thread Domains. Since 13 C spin diffusion occurs primarily along the thread axis, it provides little information on the lateral size of perfect-thread clusters or domains. This information can be obtained instead from 1 H spin diffusion. Hydrogen atoms are at the periphery of a given nanothread and therefore relatively close to 1 H in neighboring threads, so the 1 H spin diffusion between threads will be fairly fast. 1 H spin diffusion has been studied and exploited quite extensively in heterogeneous polymers, and the spin diffusion coefficient in rigid polymers is known to have a value of $D = 0.6 \pm 0.2 \text{ nm}^2/\text{ms}$. This means that, in domains of 10 nm diameter, magnetization equilibrates within about 100 ms.

Figure S9f shows cross sections, along the 13 C dimension, from 2D 1 H $-^{13}$ C HetCor spectra (Figure S9a-e) with 1 H spin diffusion during a mixing time after 1 H evolution and before the cross-polarization to 13 C. Solid lines are cross sections at a 1 H chemical shift of 6.2 ppm (alkenes), while dashed lines were obtained at 2.2 ppm (C_{β} —H) (scaled by 0.55 to

generally match at the major 80 ppm peak). Fast transfer from alkenes to alkyls generally, within 1 ms, is followed by slower spin diffusion to the perfect threads with the peaks at 77 and 50 ppm, which reaches completion within 10 ms. This slightly longer but still fairly short transfer time corresponds to perfect-thread "domains" of 1–3 nm in diameter.

DISCUSSION

Alkenes. Two types of alkene-containing rings have been identified, on the basis of distinctive cross peaks and diagonal peaks (or their absence): (i) Symmetric C—C=C—C (C_{β} = C_{β}) alkenes are found in ~24% of all C_4H_4O rings. This fully accounts for the reduced intensity of the alkyl β -carbon signal in Figure 2a and of the alkyl C_{β} — C_{β} diagonal peak in Figure 3a and suggests that these motifs dominate the nonalkyl portion of the thread backbone. Such a conclusion is further supported by the indication that the majority of these symmetric alkenes are part of a locally regular structure, with a relatively well-defined 81 ppm OCH signal and with C_{α} — C_{α} bonds connecting neighboring units, which accounts for some of the otherwise unexpected C_{α} — C_{α} diagonal intensity in Figure 3a. A distinct minority of these rings occur as defects in a variety of different environments, with a wide range of OCH chemical shifts (80–90 ppm). (ii) Asymmetric C=C—C—C $(C_{\alpha}=C_{\beta})$ alkenes are found in ~12% of all rings. Their lack of an alkyl C_{β} — C_{β} bond helps explain the reduced alkyl C_{β} — C_{β} diagonal peak in the sheared DQ/SQ NMR spectrum of Figure 3a. The asymmetric alkenes are closely associated with alkyl regions of the threads, according to the fast ¹³C spin exchange in Figure 4. Both alkene motifs can be incorporated into a thread backbone and may be associated with the initiation (asymmetric) or termination (symmetric) of nanothread polymerization via cycloaddition reactions and/or polymerization pathways that propagate a single polymerization bond chain along the thread axis, potentially via a radical polymerization pathway.⁷⁶ The presence of alkene-containing rings along the thread backbone, particularly in a locally regular structure, suggests opportunities for further functionalization, solvation, and intercalation and may suggest thread structures with intermittent alkene "hinges" between alkyl "rods", depending on the degree of completion of the thread-forming reaction. The relative ratio of alkyl and alkene components is likely amenable to experimental control through the tuning of reaction conditions.

Trapped Furan. Two unusually sharp peaks of =C-H moieties were observed at 111 and 142 ppm, close to the resonance positions of the two carbons in furan. They are directly bonded, according to cross peaks in Figure 3. The expected 111 ppm diagonal peak of two chemically equivalent β-carbons was also observed in the sheared DQ/SQ spectrum of Figure 3a. Furthermore, the 1 H chemical shifts of 7.3 and 6.3 ppm (see Figure S3) match those in furan. Thus, it is clear that these signals, which correspond to 7% of all C, arise from a trapped monomer. Incomplete dipolar dephasing (see Figure 2d) indicates large-amplitude mobility. Still, cross-polarization shows that the C-H dipolar coupling has not been averaged to zero. These furan molecules are coupled quite strongly to the immobile matrix, receiving magnetization from it via 1 H spin diffusion within 1 ms and via 13 C spin exchange on a 0.5 s time scale

Initially, two distinct sharp peaks of isotropically mobile liquid- or gas-like furan were also observed in direct-polarization ¹³C and ¹H spectra (see Figures S10 and S11).

The signals disappeared after venting the sample (i.e., opening the cap of the rotor) for a few minutes and reappeared only to a small extent over the course of 3 weeks.

The mobile furan undergoes the fastest ¹³C relaxation of all carbons in the sample (see Figure 6), which is consistent with the significant mobility of the furan molecules producing larger-amplitude fluctuating fields with spectral density at the NMR Larmor frequency. A gradual slow-down of ¹³C relaxation of the nanothreads over the course of a few weeks suggests that it is driven significantly by ¹³C spin exchange from trapped furan, whose concentration decreased with time by a few percent (of all C in the sample), in particular due to venting.

Perfect-Thread Structure. The 2D and selective 1D NMR spectra in Figures 5b and 6 show convincing evidence of the presence of ~10% of fully saturated perfect threads. These exhibit two sharp peaks, at 77 ppm of OCH and at 50 ppm of CH not bonded to O, in a 1:1 intensity ratio. The line width of 140–200 Hz is spinning-speed dependent and mostly homogeneous in nature, according to $T_{\rm 2C}$ measurements. Most of the broadening can be attributed to two or three one-bond $^{13}{\rm C}-^{13}{\rm C}$ couplings, including two $^{1}J_{\rm C-C}$ couplings of ~40 Hz. The bonding in the perfect threads documented by $^{13}{\rm C}-^{13}{\rm C}$ NMR involves multiple ${\rm C}_{\alpha}-{\rm C}_{\beta}$ bonds and a ${\rm C}_{\beta}-{\rm C}_{\beta}$ bond but no ${\rm C}_{\alpha}-{\rm C}_{\alpha}$ bond. Threads of this kind (see Figure 8) have been predicted to form by [4+2] cycloaddition.

The small number of peaks indicates a high symmetry of the perfect threads, higher than in syn/anti-threads, which contain four distinct carbon sites. Quantum-chemical calculations confirm that there is no accidental degeneracy of chemical shifts, so our data clearly rule out syn/anti- and other complex threads. Pure syn- or anti-threads are both compatible with the number of signals observed. However, syn-threads are excluded by several observations, while anti-threads can explain all the data. CODEX NMR shows that the perfect threads have at least eight C—H bond orientations, more than the four in synthreads. The OCH chemical shift in syn-threads according to DFT-based calculations is 87 ppm, which deviates by 10 ppm from the observed 77 ppm OCH signal. An even larger discrepancy of 13 ppm was found for the [2 + 2] polymer. In the 1,3-polymer, both predicted chemical shifts significantly deviated from experiment, in opposite directions.

A slower $T_{\rm 1C}$ relaxation of the perfect threads can be attributed to reduced fluctuating magnetic fields with a rate near the NMR Larmor frequency, due to smaller amplitude motions of, or near, the perfect threads. The perfect threads are more rigid than the defective threads and/or less accessible to the mobile, fast-relaxing trapped furan.

¹³C Spin Diffusion along the Nanothreads. The average length of the perfect thread segments can be determined by analyzing the ¹³C spin exchange with the surrounding imperfect segments, on a scale of several nanometers. ¹³C spin exchange along a given thread can occur relatively fast by the means of an uninterrupted sequence of strong 1.54 Å one-bond dipolar couplings of about 2 kHz in magnitude, leading to an average exchange rate of k = 80 Hz under magic-angle spinning conditions according to the CODEX decay constant (see Figure 9). The couplings between ¹³C in different threads are much weaker, given the thread center-to-center distance of 5.5 Å. At an estimated 4.5 Å closest approach of carbons in neighboring threads, the dipolar coupling strength is only 0.08 kHz, 25 times weaker than that within a thread. The truncation of the weak interthread ¹³C-¹³C couplings by the strong

intrathread ones with which their Hamiltonian does not commute further slows down interthread ¹³C spin exchange. ¹³C spin exchange or spin diffusion in nanothreads can therefore be well-approximated as a one-dimensional process along a given thread. The transition from ¹³C spin exchange to spin diffusion is discussed in the SI.

Determining the Length of Perfect-Thread Segments. Differential ¹³C inversion recovery shows that perfectand defective-thread segments are not intimately mixed. The simulations of simultaneous relaxation and spin exchange (see Figure S8a,b) show that, regardless of the intrinsic relaxation times, such a large difference (~ 2 s) in observed T_{1C} is possible only if the perfect-thread segment is at least 14 bonds in length. Considering that the 90% of defective threads are then ~126 bonds long, this result is in agreement with the 18-30bond length scale of ¹³C spin diffusion along the thread on the 1 s time scale estimated in the SI. The relatively fast intensity decrease due to spin diffusion out of the perfect threads after the zero crossing of the matrix magnetization (see Figure 7) can only be fit if the perfect-thread segment is at most 14 bonds in length. 13C spin diffusion out of the perfect thread segment also explains most of the gradual decrease of the asymptote in the CODEX decay in Figure 9. The simulated time evolutions of the magnetization distributions in all these cases are documented in Figure S8.

Accordingly, fast ¹H spin diffusion (see Figure S9) also shows that the perfect threads are near defective threads and clearly do not form large crystals. Nevertheless, some clustering of perfect threads is likely: even the random probability that one of the six neighbors of a perfect thread is also perfect exceeds 50%. The ability of furan-derived nanothread samples to produce sharp quasi-6-fold X-ray diffraction²² suggests that the alkene portions of threads have geometrical characteristics sufficiently similar to the fully saturated alkyl components that they can pack into a common well-ordered lattice.

CONCLUSIONS

¹³C-enrichment of furan by custom synthesis followed by modest-pressure synthesis of ¹³C-enriched nanothreads enabled a detailed characterization of the reaction products by a full complement of advanced solid-state NMR techniques, with validation by DFT-based calculation of chemical shifts. The ¹³C NMR spectrum was complex, with more than a dozen distinct features, but almost all (>95%) signals represented CH moieties as expected in nanothreads, with only 2-4% CH₂, 0.3% C=O, and 0.3% COO groups, according to spectral editing. Different components were quantified by integration of the fully equilibrated direct-polarization spectrum. The fraction of sp²-hybridized C was 25%, corresponding to 43% of C₄H₄O rings. Symmetric and asymmetric alkene-containing rings as well as trapped unreacted furan were identified by ¹³C-¹³C and ¹H-¹³C NMR. The most intriguing component observed was perfect fully saturated anti-nanothread segments, with two distinct sharp peaks, accounting for ca. 10% of the material. The bonding patterns in these periodic structures deduced from DQ/SQ NMR was that of a [4 + 2] cycloaddition product. While the small number of chemically inequivalent carbon sites eliminated syn/anti- and other lowsymmetry threads, the large number of magnetically inequivalent sites (i.e., distinct C-H orientations) in CODEX NMR was incompatible with the high-symmetry syn-threads. Anti-threads with two chemically and eight

magnetically inequivalent sites matched the experimental data. Quantum—chemical simulations showed good agreement of isotropic chemical shifts only for the *anti*-threads. This represents the first molecular-level identification of a specific type of nanothread. The typical length of the perfect, fully saturated thread segments was around 14–18 bonds, and they accordingly constitute small clusters (according to $^{13}\mathrm{C}$ and $^{1}\mathrm{H}$ spin diffusion analyses) that likely reside within an overall hexagonal thread packing along with other, less-perfect or less-saturated brethren. The relatively slow $T_{1\mathrm{C}}$ relaxation confirms the nanometer-scale length of the periodic perfect structure, indicates that the perfect threads are particularly rigid, and enables their selective observation in $^{13}\mathrm{C}$ NMR.

ASSOCIATED CONTENT

Supporting Information

The Supporting Information is available free of charge at https://pubs.acs.org/doi/10.1021/jacs.1c03671.

Figures of spectrally edited ¹³C NMR spectra, a CP spectrum with long recycle delay, two-dimensional ¹H-¹³C HetCor, ¹³C-¹³C exchange, and sheared DQ/SQ NMR spectra, structural model of a furan-derived thread from [4+2] cycloaddition, pulse sequence for ¹³C spin exchange after inversion recovery, plots of ¹³C spin-diffusion simulations, and ¹³C and ¹H NMR spectra; discussions of simulation of ¹³C spin exchange in CODEX NMR, transition from ¹³C spin exchange to spin diffusion, simulations of ¹³C spin diffusion, and experimental section about ¹³C₄-furan synthesis (PDF)

AUTHOR INFORMATION

Corresponding Author

Klaus Schmidt-Rohr — Department of Chemistry, Brandeis University, Waltham, Massachusetts 02453, United States; orcid.org/0000-0002-3188-4828; Email: srohr@brandeis.edu

Authors

Bryan S. Matsuura – Department of Chemistry, New York University, New York 10003, United States

Steven Huss − Department of Chemistry, The Pennsylvania State University, University Park, Pennsylvania 16802, United States; orcid.org/0000-0001-6244-4406

Zhaoxi Zheng — Department of Chemistry, Brandeis University, Waltham, Massachusetts 02453, United States Shichen Yuan — Department of Chemistry, Brandeis University, Waltham, Massachusetts 02453, United States

Tao Wang — Department of Mechanical Engineering and Department of Physics, The Pennsylvania State University, University Park, Pennsylvania 16802, United States; orcid.org/0000-0003-2833-1592

Bo Chen – Donostia International Physics Center, 20018 Donostia-San Sebastian, Spain; IKERBASQUE, Basque Foundation for Science, 48009 Bilbao, Spain; orcid.org/ 0000-0002-5084-1321

■John V. Badding — Department of Chemistry, Department of Physics, Materials Research Institute, and Department of Materials Science and Engineering, The Pennsylvania State University, University Park, Pennsylvania 16802, United States

Dirk Trauner – Department of Chemistry, New York University, New York 10003, United States; Perlmutter

- Cancer Center and NYU Neuroscience Institute, New York University School of Medicine, New York 10016, United States; © orcid.org/0000-0002-6782-6056
- Elizabeth Elacqua Department of Chemistry and Materials Research Institute, The Pennsylvania State University, University Park, Pennsylvania 16802, United States; orcid.org/0000-0002-1239-9560
- Adri C. T. van Duin Department of Mechanical Engineering, The Pennsylvania State University, University Park, Pennsylvania 16802, United States; orcid.org/ 0000-0002-3478-4945
- Vincent H. Crespi Department of Chemistry, Department of Physics, Materials Research Institute, and Department of Materials Science and Engineering, The Pennsylvania State University, University Park, Pennsylvania 16802, United States

Complete contact information is available at: https://pubs.acs.org/10.1021/jacs.1c03671

Notes

The authors declare no competing financial interest. I.V.B.: Deceased on Oct. 26, 2019.

■ ACKNOWLEDGMENTS

This work was funded by the Center for Nanothread Chemistry, a National Science Foundation (NSF) Center for Chemical Innovation (CHE-1832471). The solid-state NMR spectrometer used in this work was funded by the NSF MRI program (Award No. 1726346).

REFERENCES

- (1) Landa, S.; Machacek, V. Sur l'adamantane, nouvel hydrocarbure extrait du naphte. Collect. Czech. Chem. Commun. 1933, 5, 1-5.
- (2) Prelog, V.; Seiwerth, R. Über die Synthese des Adamantans. Ber. Dtsch. Chem. Ges. B 1941, 74 (10), 1644–1648.
- (3) Dresselhaus, M. Science of Fullerenes and Carbon Nanotubes; Elsevier, 1996; Vol. 35, p 965.
- (4) Kroto, H. W.; Heath, J. R.; O'Brien, S. C.; Curl, R. F.; Smalley, R. E. C60: Buckminsterfullerene. *Nature* **1985**, 318 (6042), 162–163.
- (5) Iijima, S. Helical microtubules of graphitic carbon. *Nature* **1991**, 354 (6348), 56–58.
- (6) Charlier, J.-C.; Blase, X.; Roche, S. Electronic and transport properties of nanotubes. *Rev. Mod. Phys.* **2007**, 79 (2), 677–732.
- (7) Golder, M. R.; Jasti, R. Syntheses of the Smallest Carbon Nanohoops and the Emergence of Unique Physical Phenomena. *Acc. Chem. Res.* **2015**, 48 (3), 557–566.
- (8) Leonhardt, E. J.; Jasti, R. Emerging applications of carbon nanohoops. *Nat. Rev. Chem.* **2019**, 3 (12), 672–686.
- (9) Van Raden, J. M.; Leonhardt, E. J.; Zakharov, L. N.; Pérez-Guardiola, A.; Pérez-Jiménez, A. J.; Marshall, C. R.; Brozek, C. K.; Sancho-García, J. C.; Jasti, R. Precision Nanotube Mimics via Self-Assembly of Programmed Carbon Nanohoops. *J. Org. Chem.* **2020**, 85 (1), 129–141.
- (10) Novoselov, K. S.; Geim, A. K.; Morozov, S. V.; Jiang, D.; Zhang, Y.; Dubonos, S. V.; Grigorieva, I. V.; Firsov, A. A. Electric field in atomically thin carbon films. *Science* **2004**, *306* (5696), 666–669.
- (11) Sofo, J. O.; Chaudhari, A. S.; Barber, G. D. Graphane: A two-dimensional hydrocarbon. *Phys. Rev. B: Condens. Matter Mater. Phys.* **2007**, 75 (15), 153401.
- (12) Wen, X. D.; Hand, L.; Labet, V.; Yang, T.; Hoffmann, R.; Ashcroft, N. W.; Oganov, A. R.; Lyakhov, A. O. Graphane sheets and crystals under pressure. *Proc. Natl. Acad. Sci. U. S. A.* **2011**, *108* (17), 6833–6837.
- (13) Strauss, M. J.; Asheghali, D.; Evans, A. M.; Li, R. L.; Chavez, A. D.; Sun, C.; Becker, M. L.; Dichtel, W. R. Cooperative Self-Assembly

- of Pyridine-2,6-Diimine-Linked Macrocycles into Mechanically Robust Nanotubes. *Angew. Chem., Int. Ed.* **2019**, 58 (41), 14708–14714.
- (14) Vitaku, E.; Gannett, C. N.; Carpenter, K. L.; Shen, L.; Abruna, H. D.; Dichtel, W. R. Phenazine-Based Covalent Organic Framework Cathode Materials with High Energy and Power Densities. *J. Am. Chem. Soc.* **2020**, *142* (1), 16–20.
- (15) Meng, Z.; Stolz, R. M.; Mirica, K. A. Two-Dimensional Chemiresistive Covalent Organic Framework with High Intrinsic Conductivity. *J. Am. Chem. Soc.* **2019**, *141* (30), 11929–11937.
- (16) Fitzgibbons, T. C.; Guthrie, M.; Xu, E.-S.; Crespi, V. H.; Davidowski, S. K.; Cody, G. D.; Alem, N.; Badding, J. V. Benzenederived carbon nanothreads. *Nat. Mater.* **2015**, *14* (1), 43–47.
- (17) Li, X.; Baldini, M.; Wang, T.; Chen, B.; Xu, E.-S.; Vermilyea, B.; Crespi, V. H.; Hoffmann, R.; Molaison, J. J.; Tulk, C. A.; Guthrie, M.; Sinogeikin, S.; Badding, J. V. Mechanochemical Synthesis of Carbon Nanothread Single Crystals. *J. Am. Chem. Soc.* **2017**, *139* (45), 16343–16349.
- (18) Li, X.; Wang, T.; Duan, P.; Baldini, M.; Huang, H.-T.; Chen, B.; Juhl, S. J.; Koeplinger, D.; Crespi, V. H.; Schmidt-Rohr, K.; Hoffmann, R.; Alem, N.; Guthrie, M.; Zhang, X.; Badding, J. V. Carbon Nitride Nanothread Crystals Derived from Pyridine. *J. Am. Chem. Soc.* 2018, 140 (15), 4969–4972.
- (19) Fanetti, S.; Santoro, M.; Alabarse, F.; Enrico, B.; Bini, R. Modulating the H-bond strength by varying the temperature for the high pressure synthesis of nitrogen rich carbon nanothreads. *Nanoscale* **2020**, *12* (8), 5233–5242.
- (20) Biswas, A.; Ward, M. D.; Wang, T.; Zhu, L.; Huang, H.-T.; Badding, J. V.; Crespi, V. H.; Strobel, T. A. Evidence for Orientational Order in Nanothreads Derived from Thiophene. *J. Phys. Chem. Lett.* **2019**, *10* (22), 7164–7171.
- (21) Nobrega, M. M.; Teixeira-Neto, E.; Cairns, A. B.; Temperini, M. L. A.; Bini, R. One-dimensional diamondoid polyaniline-like nanothreads from compressed crystal aniline. *Chem. Sci.* **2018**, 9 (1), 254–260.
- (22) Huss, S.; Wu, S.; Chen, B.; Wang, T.; Gerthoffer, M. C.; Ryan, D. J.; Smith, S. E.; Crespi, V. H.; Badding, J. V.; Elacqua, E. Scalable Synthesis of Crystalline One-Dimensional Carbon Nanothreads through Modest-Pressure Polymerization of Furan. *ACS Nano* **2021**, *15* (3), 4134–4143.
- (23) Ward, M. D.; Tang, W. S.; Zhu, L.; Popov, D.; Cody, G. D.; Strobel, T. A. Controlled Single-Crystalline Polymerization of $C_{10}H_8$. $C_{10}F_8$ under Pressure. *Macromolecules* **2019**, *52* (20), 7557–7563.
- (24) Gerthoffer, M. C.; Wu, S.; Chen, B.; Wang, T.; Huss, S.; Oburn, S. M.; Crespi, V. H.; Badding, J. V.; Elacqua, E. 'Sacrificial' supramolecular assembly and pressure-induced polymerization: toward sequence-defined functionalized nanothreads. *Chem. Sci.* **2020**, *11* (42), 11419–11424.
- (25) Friedrich, A.; Collings, I. E.; Dziubek, K. F.; Fanetti, S.; Radacki, K.; Ruiz-Fuertes, J.; Pellicer-Porres, J.; Hanfland, M.; Sieh, D.; Bini, R.; Clark, S. J.; Marder, T. B. Pressure-Induced Polymerization of Polycyclic Arene-Perfluoroarene Cocrystals: Single Crystal X-ray Diffraction Studies, Reaction Kinetics, and Design of Columnar Hydrofluorocarbons. *J. Am. Chem. Soc.* **2020**, *142* (44), 18907–18923.
- (26) Tang, W. S.; Strobel, T. A. Evidence for Functionalized Carbon Nanothreads from π -Stacked, para-Disubstituted Benzenes. *J. Phys. Chem. C* **2020**, 124 (45), 25062–25070.
- (27) Wang, Y.; Dong, X.; Tang, X.; Zheng, H.; Li, K.; Lin, X.; Fang, L.; Sun, G.; Chen, X.; Xie, L.; Bull, C. L.; Funnell, N. P.; Hattori, T.; Sano-Furukawa, A.; Chen, J.; Hensley, D. K.; Cody, G. D.; Ren, Y.; Lee, H. H.; Mao, H. K. Pressure-Induced Diels-Alder Reactions in C_6H_6 - C_6F_6 Cocrystal towards Graphane Structure. *Angew. Chem., Int. Ed.* **2019**, 58 (5), 1468–1473.
- (28) Huang, H.-T.; Zhu, L.; Ward, M. D.; Wang, T.; Chen, B.; Chaloux, B. L.; Wang, Q.; Biswas, A.; Gray, J. L.; Kuei, B.; Cody, G. D.; Epshteyn, A.; Crespi, V. H.; Badding, J. V.; Strobel, T. A. Nanoarchitecture through Strained Molecules: Cubane-Derived

- Scaffolds and the Smallest Carbon Nanothreads. J. Am. Chem. Soc. 2020, 142 (42), 17944-17955.
- (29) Roman, R. E.; Kwan, K.; Cranford, S. W. Mechanical Properties and Defect Sensitivity of Diamond Nanothreads. *Nano Lett.* **2015**, *15* (3), 1585–1590.
- (30) Silveira, J. F. R. V.; Muniz, A. R. First-principles calculation of the mechanical properties of diamond nanothreads. *Carbon* **2017**, *113*, 260–265.
- (31) Zhan, H.; Zhang, G.; Tan, V. B. C.; Cheng, Y.; Bell, J. M.; Zhang, Y.-W.; Gu, Y. From brittle to ductile: a structure dependent ductility of diamond nanothread. *Nanoscale* **2016**, *8* (21), 11177–11184.
- (32) Chen, M.-M.; Xiao, J.; Cao, C.; Zhang, D.; Cui, L.-L.; Xu, X.-M.; Long, M.-Q. Theoretical prediction electronic properties of Group-IV diamond nanothreads. *AIP Adv.* **2018**, *8* (7), 075107.
- (33) Duan, P.; Li, X.; Wang, T.; Chen, B.; Juhl, S. J.; Koeplinger, D.; Crespi, V. H.; Badding, J. V.; Schmidt-Rohr, K. The Chemical Structure of Carbon Nanothreads Analyzed by Advanced Solid-State NMR. J. Am. Chem. Soc. 2018, 140 (24), 7658–7666.
- (34) Varni, A. J.; Fortney, A.; Baker, M. A.; Worch, J. C.; Qiu, Y.; Yaron, D.; Bernhard, S.; Noonan, K. J. T.; Kowalewski, T. Photostable Helical Polyfurans. *J. Am. Chem. Soc.* **2019**, *141* (22), 8858–8867.
- (35) Varni, A. J.; Kawakami, M.; Tristram-Nagle, S. A.; Yaron, D.; Kowalewski, T.; Noonan, K. J. T. Design, synthesis, and properties of a six-membered oligofuran macrocycle. *Org. Chem. Front.* **2021**, 8 (8), 1775–1782.
- (36) Teo, Y. C.; Lai, H. W. H.; Xia, Y. Synthesis of Ladder Polymers: Developments, Challenges, and Opportunities. *Chem. Eur. J.* **2017**, 23 (57), 14101–14112.
- (37) Hou, I. C.-Y.; Hu, Y.; Narita, A.; Müllen, K. Diels-Alder polymerization: a versatile synthetic method toward functional polyphenylenes, ladder polymers and graphene nanoribbons. *Polym. J.* **2018**, *50* (1), 3–20.
- (38) Wang, T.; Duan, P.; Xu, E.-S.; Vermilyea, B.; Chen, B.; Li, X.; Badding, J. V.; Schmidt-Rohr, K.; Crespi, V. H. Constraining Carbon Nanothread Structures by Experimental and Calculated Nuclear Magnetic Resonance Spectra. *Nano Lett.* **2018**, *18* (8), 4934–4942.
- (39) Schmidt-Rohr, K.; Mao, J. D. Efficient CH-Group Selection and Identification in ¹³C Solid-State NMR by Dipolar DEPT and ¹H Chemical-Shift Filtering. *J. Am. Chem. Soc.* **2002**, *124* (46), 13938–13948.
- (40) Chen, Q.; Schmidt-Rohr, K. Backbone dynamics of the Nafion Ionomer Studied by ¹⁹F-¹³C Solid-State NMR. *Macromol. Chem. Phys.* **2007**, 208, 2189–2203.
- (41) deAzevedo, E. R.; Hu, W. G.; Bonagamba, T. J.; Schmidt-Rohr, K. Centerband-Only Detection of Exchange: Efficient Analysis of Dynamics in Solids by NMR. *J. Am. Chem. Soc.* **1999**, *121* (36), 8411–8412.
- (42) Vu, C. C.; Peterson, L. A. Synthesis of ¹³C4 furan. *J. Labelled Compd. Radiopharm.* **2005**, 48 (2), 117–121.
- (43) Oger, C.; Balas, L.; Durand, T.; Galano, J. M. Are alkyne reductions chemo-, regio-, and stereoselective enough to provide pure (Z)-olefins in polyfunctionalized bioactive molecules? *Chem. Rev.* **2013**, *113* (3), 1313–50.
- (44) Kraus, G. A.; Wang, X. An improved synthesis of 3-substituted furans from substituted butene-1,4-diols. *Synth. Commun.* **1998**, 28 (6), 1093–1096.
- (45) Qiu, J. C.; Pradhan, P. P.; Blanck, N. B.; Bobbitt, J. M.; Bailey, W. F. Selective oxoammonium salt oxidations of alcohols to aldehydes and aldehydes to carboxylic acids. *Org. Lett.* **2012**, *14* (1), 350–353.
- (46) Zhdankin, V. V.; Stang, P. J. Recent developments in the chemistry of polyvalent iodine compounds. *Chem. Rev.* **2002**, *102* (7), 2523–84.
- (47) Fang, J.; Bull, C. L.; Loveday, J. S.; Nelmes, R. J.; Kamenev, K. V. Strength analysis and optimization of double-toroidal anvils for high-pressure research. *Rev. Sci. Instrum.* **2012**, 83 (9), 093902.
- (48) Klotz, S. Techniques in high pressure neutron scattering; CRC Press, 2012; p 1-255.

- (49) Bennett, A. E.; Rienstra, C. M.; Auger, M.; Lakshmi, K. V.; Griffin, R. G. Heteronuclear Decoupling in Rotating Solids. *J. Chem. Phys.* **1995**, *103* (16), *6951–6958*.
- (50) Hahn, E. L. Spin Echoes. Phys. Rev. 1950, 80 (4), 580-594.
- (51) Dixon, W. T.; Schaefer, J.; Sefcik, M. D.; Stejskal, E. O.; McKay, R. A. Total suppression of sidebands in CPMAS C-13 NMR. *J. Magn. Reson.* (1969-1992) 1982, 49 (2), 341–345.
- (52) Fung, B. M.; Khitrin, A. K.; Ermolaev, K. An improved broadband decoupling sequence for liquid crystals and solids. *J. Magn. Reson.* **2000**, *142* (1), 97–101.
- (53) Grimmer, A.-R.; Kretschmer, A.; Cajipe, V. B. Influence of Magic Angle Spinning on Sample Temperature. *Magn. Reson. Chem.* **1997**, 35 (2), 86–90.
- (54) Chen, Q.; Hou, S.S.; Schmidt-Rohr, K. A Simple Scheme for Probehead Background Suppression in One-Pulse ¹H NMR. Solid State Nucl. Magn. Reson. **2004**, 26, 11–15.
- (55) Mao, J. D.; Schmidt-Rohr, K. Methylene spectral editing in solid-state ¹³C NMR by three-spin coherence selection. *J. Magn. Reson.* **2005**, 176 (1), 1–6.
- (56) Duan, P.; Schmidt-Rohr, K. Quick, selective NMR spectra of C-OH moieties in ¹³C-enriched solids. *J. Magn. Reson.* **2019**, 301, 80–84.
- (57) Abragam, A. The Principles of Nuclear Magnetism; Oxford University Press, 1983; p 64.
- (58) Hohwy, M.; Rienstra, C. M.; Jaroniec, C. P.; Griffin, R. G. Fivefold symmetric homonuclear dipolar recoupling in rotating solids: Application to double quantum spectroscopy. *J. Chem. Phys.* **1999**, 110 (16), 7983–7992.
- (59) Schmidt-Rohr, K. Complete Dipolar Decoupling of ¹³C and Its Use in Two-Dimensional Double-Quantum Solid-State NMR for Determining Polymer Conformations. *J. Magn. Reson.* **1998**, 131 (2), 209–17.
- (60) Caravatti, P.; Braunschweiler, L.; Ernst, R. R. Heteronuclear correlation spectroscopy in rotating solids. *Chem. Phys. Lett.* **1983**, 100 (4), 305–310.
- (61) Bielecki, A.; Kolbert, A. C.; De Groot, H. J. M.; Griffin, R. G.; Levitt, M. H. Frequency-Switched Lee—Goldburg Sequences in Solids. *Adv. Magn. Opt. Reson.* **1990**, *14*, 111–124.
- (62) ACD/Structure Elucidator, version 12.01; Advanced Chemistry Development, Inc.: Toronto, ON, Canada, 2014.
- (63) Takegoshi, K.; Nakamura, S.; Terao, T. 13 C- 1 H dipolar-assisted rotational resonance in magic-angle spinning NMR. *Chem. Phys. Lett.* **2001**, 344 (5–6), 631–637.
- (64) Pickard, C. J.; Mauri, F. All-electron magnetic response with pseudopotentials: NMR chemical shifts. *Phys. Rev. B: Condens. Matter Mater. Phys.* **2001**, 63 (24), 245101–245113.
- (65) Yates, J. R.; Pickard, C. J.; Mauri, F. Calculation of NMR chemical shifts for extended systems using ultrasoft pseudopotentials. *Phys. Rev. B: Condens. Matter Mater. Phys.* **2007**, 76 (2), 024401–024411.
- (66) Joyce, S. A.; Yates, J. R.; Pickard, C. J.; Mauri, F. A first principles theory of nuclear magnetic resonance J-coupling in solid-state systems. *J. Chem. Phys.* **2007**, *127* (20), 204107–204110.
- (67) Green, T. F. G.; Yates, J. R. Relativistic nuclear magnetic resonance J-coupling with ultrasoft pseudopotentials and the zeroth-order regular approximation. *J. Chem. Phys.* **2014**, *140* (23), 234106–234117.
- (68) Giannozzi, P.; Baroni, S.; Bonini, N.; Calandra, M.; Car, R.; Cavazzoni, C.; Ceresoli, D.; Chiarotti, G. L.; Cococcioni, M.; Dabo, I.; Dal, C. A.; Gironcoli, S.; Fabris, S.; Fratesi, G.; Gebauer, R.; Gerstmann, U.; Gougoussis, C.; Kokalj, A.; Lazzeri, M.; Martin-Samos, L.; Marzari, N.; Mauri, F.; Mazzarello, R.; Paolini, S.; Pasquarello, A.; Paulatto, L.; Sbraccia, C.; Scandolo, S.; Sclauzero, G.; Seitsonen, A. P.; Smogunov, A.; Umari, P.; Wentzcovitch, R. M. QUANTUM ESPRESSO: a modular and open-source software project for quantum simulations of materials. *J. Phys.: Condens. Matter* 2009, 21 (39), 395502–395520.
- (69) Ceresoli, D. Pseudopotentials. https://github.com/dceresoli/qe-gipaw/tree/master/pseudo (accessed 2020-12-17).

- (70) Perdew, J. P.; Burke, K.; Ernzerhof, M. Generalized Gradient Approximation Made Simple. *Phys. Rev. Lett.* **1996**, 77 (18), 3865–3868.
- (71) Charpentier, T. The PAW/GIPAW approach for computing NMR parameters: A new dimension added to NMR study of solids. *Solid State Nucl. Magn. Reson.* **2011**, 40 (1), 1–20.
- (72) Ashbrook, S. E.; McKay, D. Combining solid-state NMR spectroscopy with first-principles calculations a guide to NMR crystallography. *Chem. Commun.* **2016**, *52* (45), 7186–7204.
- (73) Ceppatelli, M.; Santoro, M.; Bini, R.; Schettino, V. High pressure reactivity of solid furan probed by infrared and Raman spectroscopy. *J. Chem. Phys.* **2003**, *118* (3), 1499–1506.
- (74) Johnson, R. L.; Anderson, J. M.; Shanks, B. H.; Fang, X.; Hong, M.; Schmidt-Rohr, K. Spectrally edited 2D ¹³C-¹³C NMR spectra without diagonal ridge for characterizing ¹³C-enriched low-temperature carbon materials. *J. Magn. Reson.* **2013**, 234, 112–24.
- (75) Schmidt-Rohr, K.; Spiess, H. W. Multidimensional Solid-State NMR and Polymers; Academic Press, 1994.
- (76) Chen, B.; Crespi, V.; Hoffmann, R.; Theoretical Studies of Furan and Thiophene Nanothreads: Structures, Cycloaddition Barriers and Activation Volumes. *ChemRxiv*, in press, **2021**.
- (77) Clauss, J.; Schmidt-Rohr, K.; Spiess, H. W. Determination of Domain Sizes in Polymers. *Acta Polym.* **1993**, 44, 1–17.